

# Render unto Numerics : Orthogonal Polynomial Neural Operator for PDEs with Non-periodic Boundary Conditions

Liu Ziyuan<sup>a</sup>, Wang Haifeng<sup>a</sup>, Bao Kaijun<sup>a</sup>, Qian Xu<sup>a</sup>, Zhang Hong<sup>a</sup>, Song Songhe<sup>a,b</sup>

<sup>a</sup>College of Science, National University of Defense Technology, Changsha 410073, China

<sup>b</sup>State Key Laboratory of High Performance Computing, National University of Defense Technology, Changsha 410073, China

---

## Abstract

By learning the map between function spaces using carefully designed deep neural networks, the operator learning become a focused field in recent several years, and have shown considerable efficiency over traditional numerical methods on solving complicated problems such as differential equations, but the method is still disturbed with the concern of its accuracy and reliability. In this paper, combined with the structures and technologies of a popular numerical method, i.e. the spectral method, a general learning-based architecture named Spectral Operator Learning is introduced. One of its variants, Orthogonal Polynomials Neural Operator designed for partial differential equations with Dirichlet, Neumann and Robin boundary conditions is proposed later, of which the effectiveness, efficacy and accuracy of boundary conditions are illustrated by numerical experiments. The code will be available after all the numerical results are summarised at [https://github.com/liu-ziyuan-math/spectral\\_operator\\_learning](https://github.com/liu-ziyuan-math/spectral_operator_learning)

*Keywords:* deep learning based PDE solver, operator learning, spectral method, orthogonal polynomials

---

## 1. Introduction

Differential equations are foundational in numerous fields of modern science and engineering, while for decades its solving have been governed by the numerical methods resulting from the fact that there is no analytic solution to most of PDEs. However, recent research shows that deep neural networks have an extraordinary capacity of solving problems with high nonlinearity and potential for constructing novel efficient approximation algorithm compared with traditional numerical methods. On the other hand, the stability and accuracy of numerical methods are ensured by numerical approximation theory, and these methods often lead to systems of sparsity, which are extremely desirable in the deployment of deep neural networks. In this paper we investigate a methodology of naturally combining both of them to propose a novel deep-learning-based framework for solving PDEs.

Denote by  $D \subset \mathbb{R}^d$  a domain. We are interested in finding a parametered approximation  $\mathcal{G}_\theta$  for the operator  $\mathcal{G} : \mathcal{A}(D; \mathbb{R}^{d_a}) \rightarrow \mathcal{U}(D; \mathbb{R}^{d_u})$ ,  $a \rightarrow u := \mathcal{G}(a)$ , where  $a \in \mathcal{A}(D; \mathbb{R}^{d_a})$  is a function. When referring to the solution operators of some given PDEs, it is essential for the approximation to satisfy the boundary conditions precisely. For example, consider the following time-dependent PDE with Neumann boundary condition:

$$\partial_t u(x, t) + \mathcal{N}(u) = 0, \quad x \in D, \quad (1)$$

---

*Email addresses:* liuziyuan17@nudt.edu.cn (Liu Ziyuan), qianxu@nudt.edu.cn (Qian Xu)

subject to

$$u(x, 0) = u_0(x), \quad x \in D, \quad (2)$$

$$\frac{\partial u}{\partial x}(x, \cdot) = 0, \quad x \in \partial D, \quad (3)$$

and denote the solution operator that evolves the wave  $u_0$  at time 0 to that at time  $t$  by  $S(t)$ , which is to say

$$u(x, t) = S(t)u_0, \quad S(t + \delta t) = S(t)S(\delta t), \quad t, \delta t \geq 0. \quad (4)$$

Let  $\mathcal{G}_\theta$  be an numerical approximation to  $S(1)$ , then the boundary condition Eq. (3) should be satisfied by the

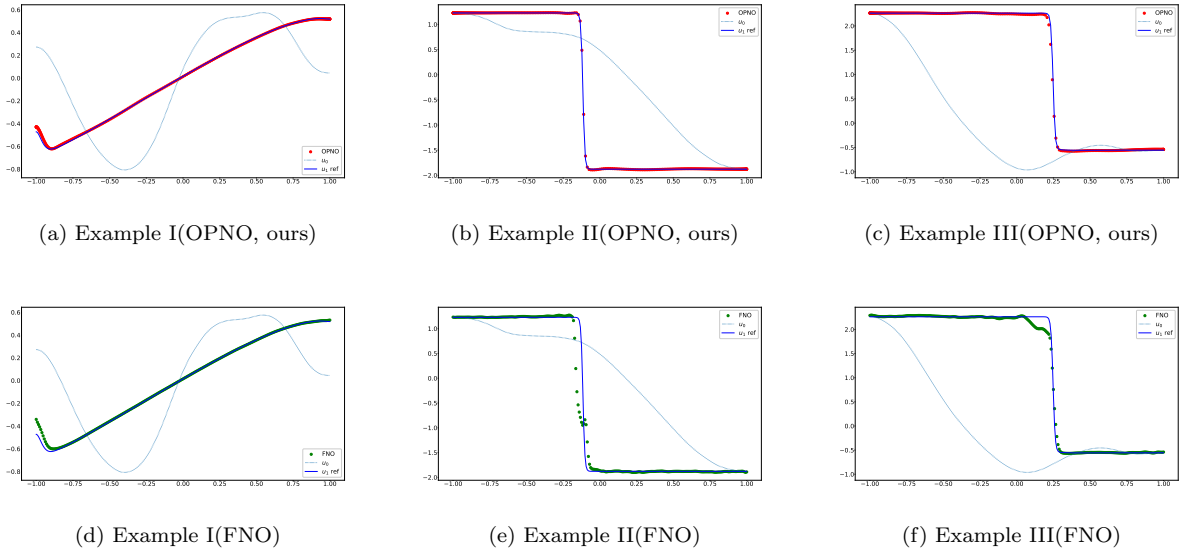


Figure 1: Numerical experiments for Burgers' equation with homogeneous Neumann condition. The dotted and solid blue lines represent initial condition  $u_0(x)$  in test datasets and the corresponding reference solution  $u_1(x)$  when  $t = 1$ , respectively. And the red dots in upper pictures are numerical solutions of our proposed OPNO method while the green dots in lower pictures are the counterparts from Fourier Neural Operators. Detailed discussion are in Sec. 4.1.

output  $\mathcal{G}_\theta(u_0)$  accurately.

The three most common types of boundary conditions in scientific and engineering computation are the Dirichlet boundary condition

$$u(x, \cdot) = f(x), \quad x \in \partial\Omega, \quad (5)$$

the Neumann boundary condition

$$\frac{\partial u}{\partial \mathbf{n}} = g(x), \quad x \in \partial\Omega, \quad (6)$$

and the Robin boundary condition

$$au(x) + b\frac{\partial u}{\partial \mathbf{n}}(x) = h(x), \quad x \in \partial\Omega, \quad (7)$$

as known as the first, second and third-type boundary condition, respectively.

Deep learning-based methods are showing promise in solving PDEs in recent several years. Some research focus on representing the solution by a neural network, such as Deep Galerkin Method [1], Deep Ritz Method [2, 3] and Physical Informed Neural Networks [4, 5], and are in theory able to overcome the curse of dimensionality. On the other hand, operator learning, a general deep-learning based methodology that learns the nonlinear mappings between function spaces are *roughly* divided into two kinds: FNO-like ones such as Fourier neural operator [6], multiwavelet-based neural operator [7], wavelet neural operator [8], and integral autoencoder [9], or DeepONet-like ones such as DeepOnet [10], DeepM&Mnet [11] and RKHS-based operators [12]. Among the operator learning methods, the Fourier neural operators are both efficient and accurate, and therefore maybe the most fruitful neural operator method till now in scientific computing and engineer, whose applications have been witnessed in high-resolution weather forecasting [13], large-scale CO2 injection simulations [14], subsurface oil/water two-phase flow simulations [15] and so on.

In this paper, based on the neural networks and spectral galerkin methods [16, 17], we discuss a general framework of Spectral Operator Learning (SOL) and then introduce a spectral operator learning method named Orthogonal Polynomial Neural Operator (OPNO) that generates numerical solution satisfying the general boundary condition mentioned above **up to a machine precision limit**. Besides, it enjoys the following desirable properties:

**Quasi-linear computation complexity.** The OPNO incurs  $O(N^d \log N)$  time complexity for  $d$ -dimensional problems owing to the application of fast cosine transform and so-called fast compacting transform.

**Efficient spatial differentiation computation.** Since the output of OPNO can be viewed as a polynomial function, its spatial difference of arbitrary order can be accurately computed within  $O(N \log N)$  operations by the method named differentiation in the frequency space (see Appendix A). Such method avoids the vanishing gradient problem in automatic differentiation of neural networks. Besides, this property leads to a zero-shot learning methodology for PDEs and will be further investigated in our future work.

**Non-overfitting training.** We have observed that as two typical examples of the Spectral Operator Learning, both FNO and OPNO are well self-regularized in solving PDEs, which means that the generalization errors will not obviously increase after long-time training, even with a small training data set.

**Quasi-spectral accuracy.** The spectral structure of SOL leads to a similar behaviour to spectral accuracy of spectral method that the model trained on a reasonably coarse meshes can be directly applied on generating solutions on fine meshes without loss of numerical accuracy, which we presume leads to the observation of resolution-invariant properties of FNO-like methods. [6, 7, 8, 18]

While only the basis of Chebyshev polynomials are discussed in detail throughout this paper, readers will find the methodology also feasible with other basis such as Legendre, Jacobi, Laguerre or Hermite polynomials and spherical harmonic functions for specific problems, e.g., those on cylindrical, spherical or unbounded domain, but we will not focus on other variants of SOL here. Furthermore, a hybrid basis could be useful for solving seperable multi-dimensional problems or coupled equations with different boundary conditions under the framework of SOL.

## 2. Spectral Operator Learning

A general spectral neural operator  $\mathcal{G}_\theta : \mathcal{A}(\Omega; R^{d_a}) \rightarrow \mathcal{U}(\Omega; R^{d_u}), a \mapsto G_\theta(a)$  is a mapping of the form

$$\mathcal{G}_\theta(a) = \mathcal{Q} \circ \mathcal{L}^{(L)} \circ \sigma \circ \mathcal{L}^{(L-1)} \circ \dots \circ \sigma \circ \mathcal{L}^{(1)} \circ \sigma \circ \mathcal{P}(a) \quad (8)$$

where  $\sigma$  is a non-polynomial activation function,  $\mathcal{Q} : \mathcal{A}(D; R^{d_a}) \rightarrow \mathcal{U}(D; R^{d_v})$  and  $\mathcal{P} : \mathcal{A}(D; R^{d_v}) \rightarrow \mathcal{U}(D; R^{d_u})$  are both local operators defined as

$$\mathcal{P}(v)(x) = Pv(x), P \in R^{d_u \times d_v}, \quad (9)$$

$$\mathcal{Q}(v)(x) = Qv(x), Q \in R^{d_u \times d_v}, \quad (10)$$

and  $\mathcal{L}^{(l)}$  are spectral linear operator layers of the form

$$\mathcal{L}^{(l)}(v) = \mathcal{T}^{-1}(A_l \cdot \mathcal{T}(v)), \quad (11)$$

where  $A_l \in R^{d_v \times d_v}$  is a (learnable) parameter linear transformation on the frequency space, and  $\mathcal{T}$  is a specific

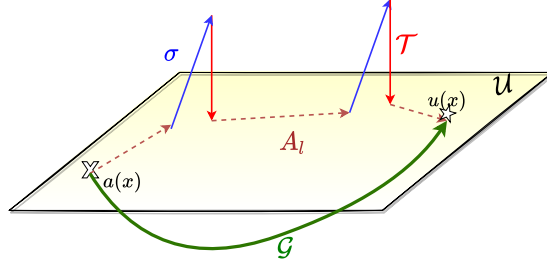


Figure 2: The sketch map for general Spectral Operator Learning

transformation operator that decomposes functions into frequency domain of corresponding basis, of which the inverse operator is denoted by  $\mathcal{T}^{-1}$ . The idea of such kind of architecture is first introduced in [6], where  $\mathcal{T} = \mathcal{F}$  (Fourier transform) is considered, and  $A_l = \text{diag}(\Lambda)$  is fixed as a diagonal matrix:

$$(\mathcal{K}(\phi)v)(x) = \mathcal{F}^{-1}(\text{diag}(\Lambda) \cdot (\mathcal{F}v))(x). \quad (12)$$

A sketch map for the Spectral Operator Learning is illustrated in Fig. 2, from which it can be figured out that the architecture of SOL is to alternately transform the function **linearly** in solution space by a spectral operator and map the function **nonlinearly** in physical space by the activation function. Readers may immediately find out the resemblance between SOL and the so-called pseudo-spectral technique which numerically solve the **linear** part of the PDE with spectral method in frequency domain, while the **nonlinear** terms are solved in physical space. What's more, the spectral linear system of SOL is designed in the same pattern of corresponding spectral methods (see Fig. 3)

While FNO is now widely applied in many problem of large scale and great complexity, most of the problem it have effectively solved are periodic, and we find that the performance of FNO drops once the periodicity is not

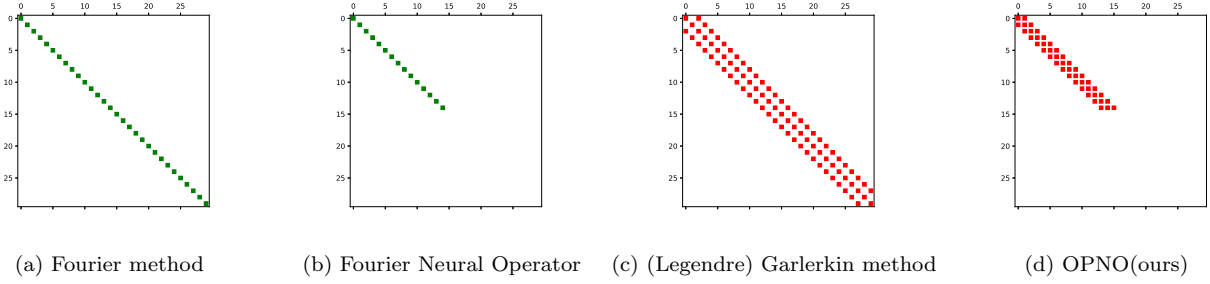


Figure 3: The spectral sparse linear systems of Fourier method, Fourier Neural Operator, spectral Galerkin method and OPNO, when solving the example boundary value problems  $\Delta u + \alpha u = 0$

assumed. For instance, [9] has showed FNO is not suitable for solving scattering problem with Sommerfeld radiation condition. Besides, since the FNO is based on the truncated basis of trigonometric polynomials, it may also be troubled with the so-called Gibbs phenomenon, which means when applying the Fourier methods to a non-periodic problem, spurious oscillations of high-frequency will be generated near the boundaries and the global convergence rate will be severely reduced (see Fig. 4). It is a common sense that for these kinds of PDEs, the spectral methods

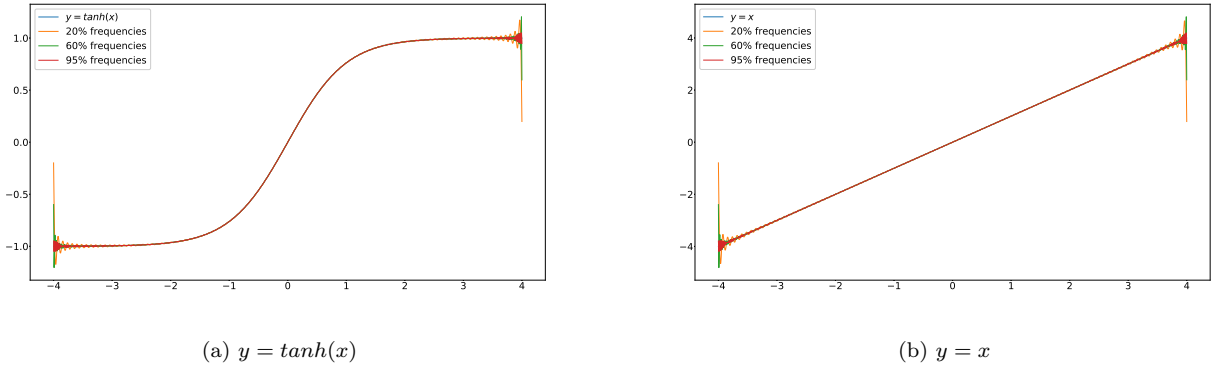


Figure 4: The truncated Fourier expansions of non-periodic functions suffer from Gibbs phenomenon. The number of discretization points is set as  $N = 1000$ .

of other kind of basis such as Chebyshev, Legendre, Jacobi, Laguerre and Hermite polynomials, rather than Fourier spectral method, should be applied [17].

Based on the spectral methods of orthogonal polynomials, especially of its compact combinations that will be introduced later, we developed the Orthogonal Polynomial Neural Operator to effectively and efficiently solve the non-periodic PDEs subject to the Dirichlet, Neumann and Robin boundary conditions. And we will focus on the Chebyshev polynomials throughout this paper.

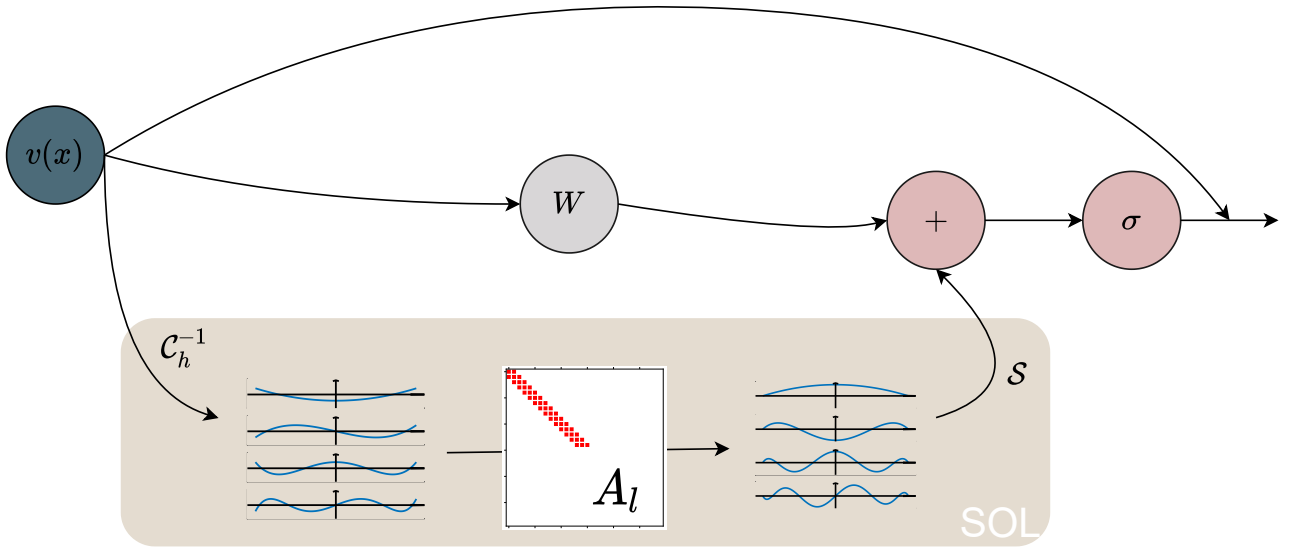


Figure 5: The architecture of the OPNO layers.

### 3. Orthogonal Polynomial Neural Operator

Without any loss of generalization, the interval  $I = [-1, 1]$  is considered, since the following method can be easily generalized to any interval  $[a, b] \subset \mathbb{R}$  by a linear map such that

$$t = x(b - a)/2 + (a + b)/2, \quad t \in [a, b]. \quad (13)$$

Based on the compact combination basis of Chebyshev polynomials  $\{\phi_k(x)\}$  Jie Shen et al. introduced in [17], we construct the fast Shen transform operator  $\mathcal{S}$  from the physical values of input function to its expansion coefficients on such basis. To fulfill this, the Fast Chebyshev Transform ( $x \rightarrow T$ ) is taken first, and then the linear mapping from Chebyshev coefficients to the coefficients of  $\phi_k$  ( $T \rightarrow \phi$ ) follows.

#### 3.1. Chebyshev transform

Chebyshev polynomials (of the first kind)  $T_n(x)$  are given by the three-term recurrence relation

$$T_{n+1}(x) = 2xT_n(x) - T_{n-1}(x), \quad n \geq 1, \quad x \in I. \quad (14)$$

To list a few,  $T_0(x) = 1$ ,  $T_1(x) = x$ ,  $T_2(x) = 2x^2 - 1$ , and  $T_3(x) = 4x^3 - 3x$ . Denote  $x_j = -\cos\frac{\pi j}{N}$ ,  $0 \leq j \leq N$  as the Chebyshev–Gauss–Lobatto points, and let  $I_N u$  be its Lagrange interpolation polynomial relative to these CGL points, then any continuous function  $u \in C[-1, 1]$  have a unique decomposition on the basis of  $T_k$ , namely

$$(I_N u)(x) = \sum_{n=0}^N \hat{u}_n T_n(x), \quad (15)$$

where  $\{\hat{u}_n\}$  are determined by the (forward) discrete Chebyshev transform  $\mathcal{C}_h$ . A more detailed introduction is given in Appendix A. The mathematical forms of forward and backward discrete Chebyshev transform are listed below.

$$\begin{aligned}
\hat{u}_n &= \frac{2}{\tilde{c}_n N} \sum_{j=0}^N \frac{1}{\tilde{c}_j} \cos \frac{nj\pi}{N}, 0 \leq n \leq N \text{ (forward transform),} \\
u(x_j) &= \sum_{n=0}^N \hat{u}_n \cos \frac{nj\pi}{N}, 0 \leq j \leq N \text{ (backward transform),}
\end{aligned} \tag{16}$$

where  $\tilde{c}_0 = \tilde{c}_N = 2$  and  $\tilde{c}_j = 1$  for  $j = 1, 2, \dots, N - 1$ .

What's more, the discrete Chebyshev transform and its inverse can be efficiently computed in  $O(N \log_2 N)$  operations via Fast Fourier Transform or Fast Cosine Transform. [19, 20]

### 3.2. Compacting operator

The compact combinations of Chebyshev polynomials  $\{\phi_k(x)\}$  is a class of basis that satisfies specific boundary conditions automatically, which is of the form

$$\phi_i(x) = T_k(x) + a_k T_{k+1}(x) + b_k T_{k+2}(x). \tag{17}$$

Consider the general (Robin) boundary condition

$$a_- u(-1) + b_- u'(-1) = 0, \quad a_+ u(1) + b_+ u'(1) = 0, \tag{18}$$

then there exists a unique set of  $\{a_k, b_k\}$  such that  $\phi_k(x)$  verifies such condition for all  $k > 0$ , which reads as follow,

$$\begin{aligned}
a_k &= 4(k+1)(a_+ b_- + a_- b_+) / DET_k, \\
b_k &= \left\{ (-2a_- a_+ + (k^2 + (k+1)^2)(a_+ b_- - a_- b_+) \right. \\
&\quad \left. + 2b_- b_+ k^2 (k+1)^2 \right\} / DET_k
\end{aligned} \tag{19}$$

where  $DET_k = 2a_+ a_- + \{(k+1)^2 + (k+2)^2\} (a_- b_+ - a_+ b_-) - 2b_- b_+ (k+1)^2 (k+2)^2$ . [17]

It is remarkable that

- For  $a_{\pm} = 1$  and  $b_{\pm} = 0$  (Dirichlet boundary conditions), we have  $\phi_k(x) = T_k(x) - T_{k+2}(x)$ .
- For  $a_{\pm} = 0$  and  $b_{\pm} = 1$  (Neumann boundary conditions), we have  $\phi_k(x) = T_k(x) - \frac{k^2}{(k+2)^2} T_{k+2}(x)$ .

The compacting operator  $\mathcal{C}_p$  is to map the Chebyshev coefficients to the expansion coefficients on  $\phi_k$  of the same function. Obviously, the compacting operator and its inverse is linear and can be carried out by recursion with  $O(N)$  operations. For example, let  $f = \sum_{j=0}^N \alpha_j T_j = \sum_{j=0}^{N-2} \beta_j \phi_j$  and consider the Dirichlet boundary condition so that  $\phi_k = T_k - T_{k+2}$ , we have

**forward compacting transform**

$$\beta_j = \begin{cases} \alpha_j, & j = 0, 1, \\ \beta_{j-2} + \alpha_j, & 2 \leq j \leq N-4, \\ -\alpha_{j+2}, & j = N-3, N-2, \end{cases} \tag{20}$$

and **backward compacting transform**

$$\alpha_j = \begin{cases} \beta_j, & j = 0, 1, \\ \beta_j - \beta_{j-2}, & 2 \leq j \leq N - 2, \\ -\beta_{j-2}, & j = N - 1, N. \end{cases} \quad (21)$$

The forward and backward compacting transform for the cases of Neumann boundary conditions are offered in Appendix B.

### 3.2.1. Fast Compacting Transform

Although the native forward compacting transform cost  $O(N)$  FLOPs theoretically, most of the coefficients need to be computed by recursion, thus it is not suitable for GPUs. Consequently, we propose a parallelable fast compacting transform. Let  $\mathbf{s}$  be a  $N$  dimensional vector with elements

$$s_n = \begin{cases} 0, & n = 2, 4, 6, \dots, \\ 1, & n = 1, 3, 5, \dots \end{cases} \quad (22)$$

Then the fast compacting transform for Eq. (20) when  $2 \leq j \leq N - 4$  is given by the discrete linear convolution of input vector  $\mathbf{x}$  and  $\mathbf{s}$ , namely

$$\mathbf{y} = \mathcal{F}^{-1}(\mathcal{F}(\bar{\mathbf{x}}) \cdot \mathcal{F}(\bar{\mathbf{s}})), \quad (23)$$

where the symbol  $\bar{\bullet}$  represents zero-padding the vector to  $2N$  length at its end (see Fig. 6). The fast compacting

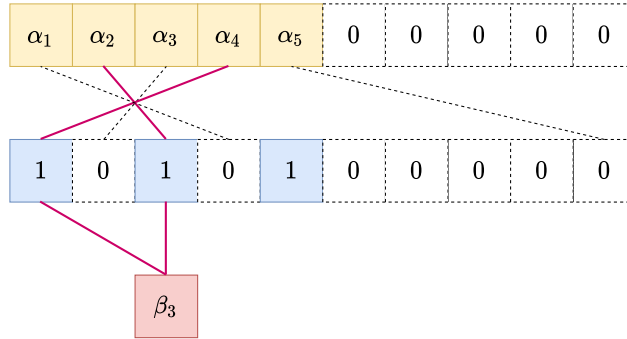


Figure 6: Schematic diagram for linear convolutions

transform exhibits about a third times improvement on the speed.

### 3.3. structure of OPNO

We finally come to the structure of OPNO. The kernel layer of OPNO is first given by substituting  $\mathcal{T}$  in Eq. (11) with  $\mathcal{S} = \mathcal{C}_p \circ \mathcal{C}_h$ .

$$\mathcal{L}_{ker}^{(l)}(v) = \mathcal{S}^{-1}(A_l \cdot \mathcal{S}(v)). \quad (24)$$



Besides, as the linear system of the Chebyshev spectral Galerkin method implies,  $A_l$  is not a diagonal matrix as FNO, but designed as quasi-diagonal with bandwidth  $w$ . We find that  $w = 3$  will suffice in the numerical examples (see Fig. 3).

Both in the kernel layers of FNO and OPNO, the matrix  $A_l$  are truncated to  $k$  modes in order to reduce the number of model parameters and focus on the low-frequency behavior of target operator. Consequently, we also add an auxiliary CNN layer  $W_l$  with 1x1 kernel in parallel to each  $\mathcal{L}_{ker}$  layer so as to capture the high-frequency part of the target operator.

As we have emphasized before, it is of significance for the numerical solution to satisfy the boundary condition accurately, so unlike the FNO, the output of OPNO is projected onto the space of  $\{\phi_k\}$  basis by the projection layer  $\mathcal{Q}$ , namely

$$\mathcal{Q}(v) = \mathcal{S}^{-1}(\mathcal{S}(Qv)), \quad (25)$$

where  $Q$  is usually shallow neural networks. Actually, to prove the convergence property of FNO for periodic problems, [21] also analysed the outputs of FNO after projected to the space of trigonometric functions, rather than the native GeLU-activated ones. We assume that the native FNO sacrifice the inherent periodic property for generalizations to non-periodic problems.

In addition, out of consideration of the efficiency, since the forward compacting operator  $\mathcal{C}_p$  is such a simple linear transform that can be easily learnt, it is omitted in all forward Shen transform except the final projection layer  $\mathcal{Q}$ . A further 2X speed optimization for the total method is witnessed and we are surprised that it even widen the application of OPNO, since by the simplification of  $\mathcal{S}$  transform the kernel layer becomes a Petrov-Galerkin-like mapping, and thus the information loss is avoided when involving non-self-adjoint problems such as odd-order equations. Lastly, we find that the skipping-connection skill of ResNet may slightly improve the performance of our model.

The architecture of OPNO is demonstrated in Eq. (26) and Fig. 5.

$$v^{(l+1)} = v^{(l)} + \sigma(W_l v^{(l)} + \mathcal{S}^{-1}(A_l \cdot \mathcal{C}_p(v^l))), \quad (26)$$

#### 4. Numerical Experiments

In this section, we compare our OPNO model with the other popular models. More experiments and operator learning models are under process. Both of the FNO and OPNO consist of 4 spectral layers with the channel width fixed as 50, and are activated by GeLU function. Since each parameter of Fourier spectral layers is complex floats representing two trigonometric polynomials of the same frequency, the Fourier and Chebyshev spectral matrix are truncated to 20 and 40 modes, respectively.

We use  $N = 1000$  training instances and 100 testing instances. To ensure the models are well trained, we use Adam optimizer to train for 5000 epochs with an initial learning rate of 0.001 that is halved every 500 epochs.

Table 1: Benchmarks on 1d Burgers equation with Neumann b.c.

N	256		1024		4096	
	$L^2$	b.c. $L^\infty$	$L^2$	b.c. $L^\infty$	$L^2$	b.c. $L^\infty$
FNO	$1.31 \times 10^{-2}$	$3.02 \times 10^{-1}$	$1.28 \times 10^{-2}$	$4.58 \times 10^{-1}$	$1.32 \times 10^{-2}$	$8.87 \times 10^{-1}$
OPNO	$7.647 \times 10^{-3}$	$5.701 \times 10^{-12}$	$7.649 \times 10^{-3}$	$1.232 \times 10^{-10}$	$7.654 \times 10^{-3}$	$1.803 \times 10^{-9}$

Notice that the FNO has been equipped with the GeLU function and latest padding strategy for non-periodic cases that is recently proposed on its Github pages.

#### 4.1. 1d burgers' equation

We consider the one-dimensional burgers' equation

$$\partial_t u(x, t) + \frac{1}{2} \partial_x (u^2(x, t)) = \nu \partial_{xx} (u, t), \quad x \in [-1, 1], \quad (27)$$

subject to the homogenous Neumann boundary conditions

$$\frac{\partial u}{\partial x}(\pm 1, \cdot) = 0. \quad (28)$$

For a fixed viscosity coefficient  $\nu$ , we aim to learn the solution operator  $S(1) : S(1)u_0 \rightarrow u(\cdot, 1), u_0 \in H_0^1(I)$ , which has been introduced in Eq. (4).

The initial condition  $u_0(x)$  is generated according to  $u_0 \sim \mu$  where  $\mu = \mathcal{N}(0, 25^2(-4\Delta + 25I)^{-2})$  with Neumann boundary conditions, and the viscosity is set as  $\nu = 0.1/\pi$  and the reference solutions are generated by chebyshev spectral method, so the dataset is comparable to the experiments of 1d burgers equation of [6] to some extent. The OPNO and FNO are trained and tested on Chebyshev-Gauss-Lobatto grids and uniform grids, respectively, and both of them are activated by the GeLU functions. The global relative  $L^2$  norm error and the  $L^\infty$  norm error to the boundary conditions (28) are performed in Tab. 1, where the boundary error of OPNO is computed by the method of differentiation in frequency space, and that of FNO is approximated the finite difference with the another nearest discretization points, i.e.

$$E_{b.c.} = \max\{|\delta_x u_1|, |\delta_x u_N|\} = \max\left\{\left|\frac{u_2 - u_1}{\Delta x}\right|, \left|\frac{u_N - u_{N-1}}{\Delta x}\right|\right\} \quad (29)$$

the OPNO outperforms the FNO not only in the errors of boundary condition but also the global approximation errors.

## Appendix A. Chebyshev polynomials

As the well-known Weierstrass approximation theorem states, any continuous function  $u(x) \in C([a, b])$  can be uniformly approximated as closely as desired by a polynomial function. Besides, among the polynomial-based methods, the Chebyshev polynomials are pretty popular in numerical approximation and simulations.

Chebyshev polynomials (of the first kind)  $T_n(x)$  are given by the three-term recurrence relation

$$T_{n+1}(x) = 2xT_n(x) - T_{n-1}(x), \quad n \geq 1, \quad x \in I. \quad (\text{A.1})$$

Fortunately, they have the explicit form of

$$T_n(x) = \cos n\theta, \quad \theta = \arccos(x), \quad x \in I, \quad (\text{A.2})$$

from which we can easily derive the following properties

$$T_n(\pm 1) = (\pm 1)^n, \quad T'_n(\pm 1) = (\pm 1)^{n-1}n, \quad (\text{A.3})$$

$$\int_{-1}^1 T_n(x)T_m(x) \frac{1}{\sqrt{1-x^2}} dx = \frac{c_n\pi}{2} \delta_{mn} \text{ (Orthogonality)}, \quad (\text{A.4})$$

$$T'_n(x) = 2n \sum_{\substack{k=0 \\ k+n \text{ odd}}}^{n-1} \frac{1}{c_k} T_k(x), \quad (\text{A.5})$$

where  $c_0 = 2$  and  $c_n = 1$  for  $n \geq 1$ . So the Chebyshev polynomials are orthogonal with respect to the weight function  $\omega(x) = (1-x^2)^{-1/2}$ .

Denote  $P^N(I)$  as the space of all polynomials in  $I$  of the degree no greater than  $N$ . For the Chebyshev-Gauss-Lobatto (CGL) quadrature, the Chebyshev-Gauss-type nodes and weights are set as

$$x_j = -\cos \frac{\pi j}{N}, \quad \omega_j = \frac{\pi}{c_j N}, \quad 0 < j \leq N, \quad (\text{A.6})$$

where  $c_j = 1$  for  $j = 1, 2, \dots, N-1$  but  $c_0 = c_N = 2$ . As a consequence, the following equation holds

$$\int_{-1}^1 p(x) \frac{1}{\sqrt{1-x^2}} dx = \sum_{j=0}^N p(x_j) \omega_j, \quad \forall p \in P_{2N-1}. \quad (\text{A.7})$$

For  $u(x) = \sum_{k=0}^N \hat{u}_k T_k(x) \in P_N(I)$ , its derivatives  $u' = \sum_{k=0}^{N-1} \hat{u}_k^{(1)} T_k(x)$  is given by the differentiation on the frequency space, namely

$$\begin{aligned} \hat{u}_{N-1}^{(1)} &= 2N\hat{u}_N, \\ \hat{u}_{k-1}^{(1)} &= (2k\hat{u}_k + \hat{u}_{k+1}^{(1)})/c_{k-1}, \quad k = N-1, \dots, 1, \end{aligned} \quad (\text{A.8})$$

which can also be calculated by a linear convolution in  $O(N \log N)$  operations.

## Appendix B. The fast compacting transform for Neumann conditions

For the compact combination  $\phi_k(x) = T_k(x) - \frac{k^2}{(k+2)^2} T_{k+2}$ , we have

**forward compacting transform**

$$\beta_j = \begin{cases} \alpha_j, & j = 0, 1, \\ p_j \beta_{j-2} + \alpha_j, & 2 \leq j \leq N-4, \\ -\frac{1}{p_j} \alpha_{j+2}, & j = N-3, N-2, \end{cases} \quad (\text{B.1})$$

and **backward compacting transform**

$$\alpha_j = \begin{cases} \beta_j, & j = 0, 1, \\ \beta_j - p_j \beta_{j-2}, & 2 \leq j \leq N-2, \\ -p_j \beta_{j-2}, & j = N-1, N, \end{cases} \quad (\text{B.2})$$

where  $p_{j+2} = j^2/(j+2)^2, 0 \leq j \leq N-2$ .

The only part that would cause trouble in parallel computing is the forward transform with  $2 \leq j \leq N-2$ . However let  $\tilde{a}_j = j^2 a_j, \tilde{b}_j = j^2 b_j$ , then this part is equivalent to the following equation

$$\tilde{\beta}_j = \tilde{\beta}_j + \tilde{a}_j, \quad 2 \leq j \leq N-2, \quad (\text{B.3})$$

thus can also be efficiently computed by the linear convolution.

## References

- [1] J. Sirignano, K. Spiliopoulos, Dgm: A deep learning algorithm for solving partial differential equations, *Journal of computational physics* 375 (2018) 1339–1364.
- [2] B. Yu, et al., The deep ritz method: a deep learning-based numerical algorithm for solving variational problems, *Communications in Mathematics and Statistics* 6 (1) (2018) 1–12.
- [3] Y. Liao, P. Ming, Deep nitsche method: Deep ritz method with essential boundary conditions, *arXiv preprint arXiv:1912.01309* (2019).
- [4] M. Raissi, P. Perdikaris, G. E. Karniadakis, Physics-informed neural networks: A deep learning framework for solving forward and inverse problems involving nonlinear partial differential equations, *Journal of Computational physics* 378 (2019) 686–707.
- [5] S. Wang, S. Sankaran, P. Perdikaris, Respecting causality is all you need for training physics-informed neural networks, *arXiv preprint arXiv:2203.07404* (2022).
- [6] Z. Li, N. Kovachki, K. Azizzadenesheli, B. Liu, K. Bhattacharya, A. Stuart, A. Anandkumar, Fourier neural operator for parametric partial differential equations, *arXiv preprint arXiv:2010.08895* (2020).
- [7] G. Gupta, X. Xiao, P. Bogdan, Multiwavelet-based operator learning for differential equations, *Advances in Neural Information Processing Systems* 34 (2021) 24048–24062.
- [8] T. Tripura, S. Chakraborty, Wavelet neural operator: a neural operator for parametric partial differential equations, *arXiv preprint arXiv:2205.02191* (2022).
- [9] Y. Z. Ong, Z. Shen, H. Yang, Iae-net: Integral autoencoders for discretization-invariant learning, *arXiv preprint arXiv:2203.05142* (2022).

- [10] L. Lu, P. Jin, G. E. Karniadakis, Deeponet: Learning nonlinear operators for identifying differential equations based on the universal approximation theorem of operators, arXiv preprint arXiv:1910.03193 (2019).
- [11] S. Cai, Z. Wang, L. Lu, T. A. Zaki, G. E. Karniadakis, Deepm&mnet: Inferring the electroconvection multiphysics fields based on operator approximation by neural networks, *Journal of Computational Physics* 436 (2021) 110296.
- [12] K. Bao, X. Qian, Z. Liu, H. Wang, S. Song, Function-valued rkhs-based operator learning for differential equations, arXiv preprint arXiv:2202.09488 (2022).
- [13] J. Pathak, S. Subramanian, P. Harrington, S. Raja, A. Chattopadhyay, M. Mardani, T. Kurth, D. Hall, Z. Li, K. Azizzadenesheli, et al., Fourcastnet: A global data-driven high-resolution weather model using adaptive fourier neural operators, arXiv preprint arXiv:2202.11214 (2022).
- [14] T. J. Grady, R. Khan, M. Louboutin, Z. Yin, P. A. Witte, R. Chandra, R. J. Hewett, F. Herrmann, Model-parallel fourier neural operators as learned surrogates for large-scale parametric pdes, 2022.
- [15] K. Zhang, Y. Zuo, H. Zhao, X. Ma, J. Gu, J. Wang, Y. Yang, C. Yao, J. Yao, Fourier neural operator for solving subsurface oil/water two-phase flow partial differential equation, *SPE Journal* (2022) 1–15.
- [16] J. Shen, Efficient spectral-galerkin method ii. direct solvers of second-and fourth-order equations using chebyshev polynomials, *SIAM Journal on Scientific Computing* 16 (1) (1995) 74–87.
- [17] J. Shen, T. Tang, L.-L. Wang, *Spectral methods: algorithms, analysis and applications*, Vol. 41, Springer Science & Business Media, 2011.
- [18] S. Cao, Choose a transformer: Fourier or galerkin, *Advances in Neural Information Processing Systems* 34 (2021) 24924–24940.
- [19] L. N. Trefethen, *Spectral methods in MATLAB*, SIAM, 2000.
- [20] C. Wen-Hsiung, C. Smith, S. Fralick, A fast computational algorithm for the discrete cosine transform, *IEEE Transactions on Communications* 25 (9) (1977) 1004–1009.
- [21] N. Kovachki, S. Lanthaler, S. Mishra, On universal approximation and error bounds for fourier neural operators, *Journal of Machine Learning Research* 22 (2021) Art–No.